Bond Length and Local Energy Density Property Connections for Non-Transition-Metal Oxide-Bonded Interactions

G. V. Gibbs,*,† M. A. Spackman,‡ D. Jayatilaka,‡ K. M. Rosso,§ and D. F. Cox||

Department of Geosciences, Materials Science, and Engineering and Mathematics, Virginia Tech, Blacksburg, Virginia 24061, School of Biomedical, Biomolecular and Chemical Sciences, University of Western Australia, Crawley WA 6009, Australia, William R. Wiley Environmental Molecular Sciences Laboratory, Pacific Northwest National Laboratories, Richland, Washington 99352, and Department of Chemical Engineering, Virginia Tech, Blacksburg, Virginia 24061

Received: May 16, 2006; In Final Form: August 29, 2006

For a variety of molecules and earth materials, the theoretical local kinetic energy density, $G(\mathbf{r}_c)$, increases and the local potential energy density, $V(\mathbf{r}_c)$, decreases as the M−O bond lengths (M = first- and second-row metal atoms bonded to O) decrease and the electron density, $\rho(\mathbf{r}_c)$, accumulates at the bond critical points, $\mathbf{r}_c$. Despite the claim that the local kinetic energy density per electronic charge, $G(\mathbf{r}_c)/\rho(\mathbf{r}_c)$, classifies bonded interactions as shared interactions when less than unity and closed-shell when greater, the ratio was found to increase from 0.5 to 2.5 au as the local electronic energy density, $H(\mathbf{r}_c) = G(\mathbf{r}_c) + V(\mathbf{r}_c)$, decreases and becomes progressively more negative. The ratio appears to be a measure of the character of a given M−O bonded interaction, the greater the ratio, the larger the value of $\rho(\mathbf{r}_c)$, the smaller the coordination number of the M atom and the more shared the bonded interaction. $H(\mathbf{r}_c)/\rho(\mathbf{r}_c)$ versus $G(\mathbf{r}_c)/\rho(\mathbf{r}_c)$ scatter diagrams categorize the M−O bonded interactions into domains with the local electronic energy density per electron charge, $H(\mathbf{r}_c)/\rho(\mathbf{r}_c)$, tending to decrease as the electronegativity differences for the bonded pairs of atoms decrease. The values of $G(\mathbf{r}_c)$ and $V(\mathbf{r}_c)$, estimated with a gradient-corrected electron gas theory expression and the local virial theorem, are in good agreement with theoretical values, particularly for the bonded interactions involving second-row M atoms. The agreement is poorer for shared C−O and N−O bonded interactions.

Introduction

During the latter part of the last century, two important strategies were forged for studying and classifying the bonded interactions of a material in terms of the bond critical point and the local density properties displayed by an electron density distribution, $\rho(\mathbf{r})$. The one proposed by Bader and Essén[1] is based on the accumulation of the electron density, $\rho(\mathbf{r}_c)$, and the sign and magnitude of the Laplacian, $\nabla^2\rho(\mathbf{r}_c) = 4(2G(\mathbf{r}_c) + V(\mathbf{r}_c))$, at the bond critical point, $\mathbf{r}_c$, of a bonded interaction where the local kinetic energy density, $G(\mathbf{r}_c)$, is always positive and the local potential energy density, $\boldsymbol{V}(\mathbf{r}_c)$, is always negative. When $|V(\mathbf{r}_c)| > 2G(\mathbf{r}_c)$ such that $\nabla^2\rho(\mathbf{r}_c)$ is negative and the value of $\rho(\mathbf{r}_c)$ is relatively large, a shared interaction is indicated, but when $2G(\mathbf{r}_c) > |V(\mathbf{r}_c)|$ such that $\nabla^2\rho(\mathbf{r}_c)$ is positive, an interaction is indicated to be either intermediate or closed-shell, depending on the proximity of $\mathbf{r}_c$ to the $\nabla^2\rho(\mathbf{r}) = 0$ nodal surface of the Laplacian. When $\mathbf{r}_c$ is distant from the surface, the interaction is indicated to be closed-shell, but when it is in close proximity, the interaction is indicated to be intermediate in character, such that the closer that $\mathbf{r}_c$ is to the surface, the more shared the interaction.

The second classification, proposed by Cremer and Kraka,[2] is also based on the accumulation of the electron density at $\mathbf{r}_c$, but rather than being based on the sign of $\nabla^2\rho(\mathbf{r}_c)$, it is based on the sign of the local electronic energy density, $H(\mathbf{r}_c) = G(\mathbf{r}_c) + V(\mathbf{r}_c)$. When $|V(\mathbf{r}_c)| > G(\mathbf{r}_c)$ and $H(\mathbf{r}_c)$ is negative, the bonded interaction is indicated to be shared, but when $G(\mathbf{r}_c) > |V(\mathbf{r}_c)|$ and $H(\mathbf{r}_c)$ is positive, the interaction is indicated to be closed-shell. In general, the larger the value of $|V(\mathbf{r}_c)|$ and the more negative the value of $H(\mathbf{r}_c)$, the more shared the bonded interaction and the greater the stabilization of the structure. Both strategies have been used with varying degrees of success but neither has been found to be universal in its application.

Early this century, a third classification by Espinosa et al.[3] was proposed on the basis of the bond degree $|V(\mathbf{r}_c)|/G(\mathbf{r}_c)$ ratio rather than on $\nabla^2\rho(\mathbf{r}_c)$ and $H(\mathbf{r}_c)$ individually. It was assumed, as asserted by Cremer and Kraka,[2] that an interaction is closed-shell when $H(\mathbf{r}_c) \geq 0$ and that it is shared when $\nabla^2\rho(\mathbf{r}_c) \leq 0$, as asserted by Bader and Essén.[1] For the case where $H(\mathbf{r}_c) = 0$, $G(\mathbf{r}_c) + V(\mathbf{r}_c) = 0$ and for the case where $\nabla^2\rho(\mathbf{r}_c) = 0$, $2G(\mathbf{r}_c) + V(\mathbf{r}_c) = 0$, the two equalities $|V(\mathbf{r}_c)|/G(\mathbf{r}_c) = 1$ and $|V(\mathbf{r}_c)|/G(\mathbf{r}_c) = 2$ each hold, respectively. With these equalities, a bonded interaction is indicated to be closed-shell when the ratio $|V(\mathbf{r}_c)|/G(\mathbf{r}_c) < 1$, shared when $|V(\mathbf{r}_c)|/G(\mathbf{r}_c) > 2$, and intermediate when the ratio falls in the range between 1 and 2.

A survey of the literature shows that all three classifications have the merits of being straightforward, easy to apply, and useful in advancing our understanding of the bonded interactions for a variety of materials.[4] The Bader and Essén[1] classification

* Author to whom correspondence should be addressed. E-mail: gvgibbs@vt.edu.
† Department of Geosciences, Materials Science, and Engineering and Mathematics, Virginia Tech.
‡ University of Western Australia.
§ Pacific Northwest National Laboratories.
|| Department of Chemical Engineering, Virginia Tech.

10.1021/jp062992m CCC: $33.50
Published on Web 10/18/2006

does an adequate job evaluating and classifying the bonded interactions particularly for a wide range of diatomic molecules and materials consisting of first-row atoms but, as discussed below, it may be inadequate for the classification of transition-metal-bonded interactions.[5−9] There may also be a problem when the bond critical point, $\mathbf{r}_c$, is located in close proximity with the nodal surface of $\nabla^2\rho(\mathbf{r})$ where $\nabla(\nabla^2\rho(\mathbf{r}))$ may be large to the extent that the inaccuracy of the determination of $\nabla^2\rho(\mathbf{r}_c)$ is potentially large.[10]

The Cremer and Kraka[2] classification considers a bonded interaction as either closed-shell or shared, but it does not provide a classification for bonded interactions of intermediate character. Nonetheless, for a given shared bonded interaction, $H(\mathbf{r}_c)$ is indicated to be negative and to decrease in a regular way with increasing shared character and, as such, can provide a straightforward and adequate method for determining whether a given bonded interaction has a greater component of shared character than another.

Although new and not thoroughly tested, the $|V(\mathbf{r}_c)|/G(\mathbf{r}_c)$ ratio[3] has provided an adequate classification for a variety of M−X (X = O, F) and M−M bonded interactions,[11,12] but as discussed in more detail below, it does not appear to manifest a change in the character of a bonded interaction as the coordination number and the net atomic charge conferred on a bonded atom decrease and as $\rho(\mathbf{r}_c)$ increases in value.[13]

In the current study, the three classifications together with the ratios $G(\mathbf{r}_c)/\rho(\mathbf{r}_c)$ and $H(\mathbf{r}_c)/\rho(\mathbf{r}_c)$ will be examined for a relatively large number of non-transition-metal oxygen M−O bonded interactions in terms of their experimental and theoretical bond lengths. For reasons that are not entirely clear, it is generally accepted that the local kinetic energy per electronic charge, $G(\mathbf{r}_c)/\rho(\mathbf{r}_c)$, is less than unity for shared interactions and greater than unity for closed-shell interactions.[1,8,14] However, for a large number of earth materials and several molecules, a connection will be examined between the M−O bond length, R(M−O), and the $G(\mathbf{r}_c)/\rho(\mathbf{r}_c)$ ratio that suggests that the ratio actually exceeds unity for several shared bonded interactions such as the shared triple C≡O bonded interaction for the carbon monoxide molecule.[8] A second connection between R(M−O) and the local electronic energy per electronic charge, $H(\mathbf{r}_c)/\rho(\mathbf{r}_c)$, indicates that the ratio may be related to some intrinsic property such as the electronegativity difference and the shared character of the bonded M and O atoms.[3] Finally, the theoretical local kinetic and potential energy densities will be compared with those estimated with an expression on the basis of the gradient-corrected electron gas theory and the local virial theorem.

Local Energy Density Properties for Earth Materials and Molecules. In an exploration of how the local energy density properties vary with bond length for a variety of M−O bonded interactions (where the M-atom represents the first-row atom sequence Be to N and the second-row sequence from Na to S, each bonded to O), the properties were calculated for molecules and a large number of earth materials.[13] The calculations for the crystalline earth materials were completed with CRYSTAL98[15] and TOPOND[16] and those for C−O and N−O bond-bearing molecules were completed with GAUSSIAN98 at the BLYP/6-311++G(2d,p) level.[13] The electron density distribution for each crystal was computed using Bloch functions expanded as linear combinations of atomic centered Gaussian basis sets. Self-consistent field wave functions, solved in reciprocal space, were computed for each structure at the density functional theory level, using the local density approximation for the exchange potential[17] and the Vosko−Wilk−Nusair[18] parametrization of the correlation potential. Further, the basis sets used in the calculations, as described in more detail elsewhere,[19,20] were specifically optimized for the atoms comprising each crystal. The bond critical point and the local energy density properties for the theoretical electron density distributions for the crystals were generated with TOPOND, kindly supplied for our use by Professor Carlo Gatti. Those for the molecules were generated with software kindly supplied by Professor Richard Bader.

The results of the calculations embody a range of properties for each M−O bonded interaction that provide a basis for exploring how the properties vary with the experimental and geometry optimized M−O bond lengths and Allen's spectroscopic electronegativity differences, $\Delta\chi$, for the bonded atoms M and O.[21] An earlier calculation of the bond critical point properties for many earth materials shows that as the magnitudes of $\nabla^2\rho(\mathbf{r}_c)$, $\rho(\mathbf{r}_c)$, and the three curvatures of $\rho(\mathbf{r}_c)$, λ_i, each increase and the bonded radii of the M and O atoms and $\Delta\chi$ decrease, the M−O bond lengths decrease. As these results have been reported and examined elsewhere,[19,20] they will not be examined further here.

With the calculated local energy density properties, scatter diagrams were prepared to explore the connection between R(M−O) and $G(\mathbf{r}_c)$, $V(\mathbf{r}_c)$, $G(\mathbf{r}_c)/\rho(\mathbf{r}_c)$, $H(\mathbf{r}_c)/\rho(\mathbf{r}_c)$, and so forth to learn whether meaningful connections emerge for a relatively wide range of M−O bonded interactions that may add to our understanding of the local energy density properties. In addition, diagrams for $G(\mathbf{r}_c)/\rho(\mathbf{r}_c)$ versus $H(\mathbf{r}_c)/\rho(\mathbf{r}_c)$ and $|V(\mathbf{r}_c)|/G(\mathbf{r}_c)$ versus $H(\mathbf{r}_c)/\rho(\mathbf{r}_c)$ will be generated to explore how well the bonded interactions involving different M atoms bonded to O can be categorized. It will be of interest to learn the extent to which the ratios $G(\mathbf{r}_c)/\rho(\mathbf{r}_c)$ and $H(\mathbf{r}_c)/\rho(\mathbf{r}_c)$ categorize the bonded interactions into discrete classes, for example, and whether the ratio $|V(\mathbf{r}_c)|/G(\mathbf{r}_c)$ classifies the M−O bonded interactions for non-transition-metal oxides in a self-consistent way. It will also be of interest to learn whether a connection exists between the ratios $G(\mathbf{r}_c)/\rho(\mathbf{r}_c)$ and $H(\mathbf{r}_c)/\rho(\mathbf{r}_c)$ and the properties of the bonded atoms. Last, we will examine the extent to which the values for local potential and kinetic energy densities generated in our calculations match those estimated, using an expression on the basis of the gradient-corrected electron gas theory,[22] the $\rho(\mathbf{r}_c)$ and $\nabla^2\rho(\mathbf{r}_c)$ values obtained in our calculations, and the local virial theorem.

Scatter Diagrams. The local kinetic energy density, $G(\mathbf{r}_c)$, evaluated for the earth materials and molecules, is plotted against R(M−O) Å in Figure 1a. As observed for both $\rho(\mathbf{r}_c)$ and $\nabla^2\rho(\mathbf{r}_c)$, $G(\mathbf{r}_c)$ increases nonlinearly along two separate power law like trends with decreasing bond length, the lower trend in the figure consists of bonded interactions that involve first-row M atoms bonded to O and the upper consists of interactions that involve second-row M atoms bonded to O.[19] The increase in $G(\mathbf{r}_c)$ with decreasing bond length is expected, given that the values of $\rho(\mathbf{r}_c)$ and $\nabla^2\rho(\mathbf{r}_c)$ both increase and that $\nabla^2\rho(\mathbf{r}_c)$ is largely positive, particularly for the second-row M atoms. Thus, as the local kinetic energy of the bonded interactions increases, $\rho(\mathbf{r})$ is progressively accumulated and locally concentrated at $\mathbf{r}_c$. Accordingly, shorter M−O bonds not only embody larger local kinetic energy density values at $\mathbf{r}_c$, but they are indicated to have more shared character than those with smaller local kinetic energy density values given that $G(\mathbf{r}_c)$ tends to increase as $\Delta\chi$[21] decreases and $\rho(\mathbf{r})$ increases in value.[23]

On the basis of the local virial theorem, $1/4\nabla^2\rho(\mathbf{r}_c) = 2G(\mathbf{r}_c) + V(\mathbf{r}_c)$, Bader[14] "anticipated" that the local kinetic energy density per electronic charge, $G(\mathbf{r})/\rho(\mathbf{r}_c)$, is less than unity for

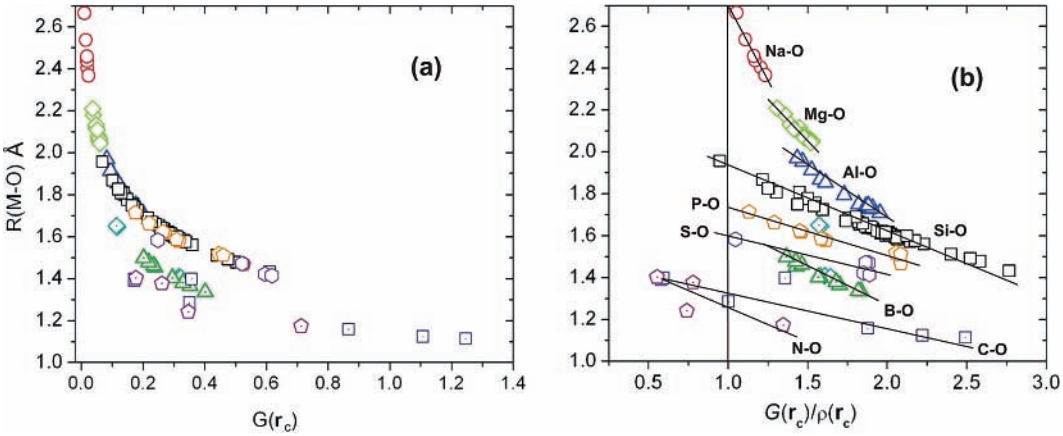

Figure 1. Scatter diagrams of the observed bond lengths, R(M−O) Å, for a relatively large number of earth materials and geometry optimized bond lengths for molecules with C−O and N−O bonded interactions plotted against (a) the local kinetic energy $G(\mathbf{r}_c)$ (au) calculated with TOPOND for the crystals and with EXTREM for the molecules and (b) the ratio $G(\mathbf{r}_c)/\rho(\mathbf{r}_c)$ where $\rho(\mathbf{r}_c)$ is the value of the $\rho(\mathbf{r})$ at the bond critical point, $\mathbf{r}_c$. The red circles represent Na−O bonded interactions, the green diamond Mg−O, the blue triangle Al−O, the black square Si−O, the orange pentagon P−O, the violet hexagon S−O, the dot-centered dark cyan diamond Be−O, the dot-centered olive triangle B−O, the dot-centered navy square C−O, and the dot-centered purple pentagon N−O.

shared bonded interactions and greater than unity for closed-shell interactions. The $G(\mathbf{r})/\rho(\mathbf{r}_c)$ ratio is plotted for the M−O bonded interactions against. R(M−O) in Figure 1b. For each interaction, the ratio increases linearly with decreasing bond length. The ratios for the Na−O and Mg−O bonded interactions are greater than unity and, as expected, classify as closed-shell. In addition, the ratios for the single C−O and N−O bonded interactions are less than unity and, as expected, classify as shared. However, the ratios for the remaining M−O bonded interactions are greater than unity and classify as closed-shell, including the double C═O bonded interaction for carbon dioxide and the triple C≡O interaction for carbon monoxide.

For each bonded interaction, as $G(\mathbf{r})/\rho(\mathbf{r}_c)$ increases, not only do the M−O bond lengths decrease but, as expected, the coordination numbers of the M atoms decrease. The coordination number of an M atom, ν_M, denoted by a Roman numerical superscript, is attached to the atomic symbol for convenience of discussion. In the case of the B−O bonded interactions, as $G(\mathbf{r})/\rho(\mathbf{r}_c)$ increases in value from ∼1.5 to ∼2.0 au, the coordination numbers of the B atoms comprising the tetrahedral $^{IV}BO_4$ and triangular $^{III}BO_3$ coordinated polyhedra decrease from 4 to 3, respectively, as R(B−O) decreases from 1.45 Å to 1.35 Å. A similar trend holds for the bulk of the remaining bonded interactions with the lengths of the bonds and the coordination numbers of the M atoms decreasing as $G(\mathbf{r})/\rho(\mathbf{r}_c)$ increases. For example, as the ratio for the Al−O bonded interaction increases from ∼1.5 to ∼2.0 au, R(Al−O) decreases in succession from R(^{VI}Al−O) ∼ 1.95 Å to R(^{V}Al−O) ∼ 1.85 Å to R(^{IV}Al−O) ∼ 1.75 Å, respectively. In addition, as the ratio increases from ∼1.0 to ∼2.7 au, R(Si−O) decreases from R(^{VI}Si−O) ∼ 1.75 Å to R(^{IV}Si−O) ∼ 1.62 Å and as the ratio increases from ∼0.5 to 2.5 au, R(C−O) decreases from R(^{IV}C−O) = 1.39 Å to R(^{III}C−O) = 1.29 Å to R(^{II}C−O) = 1.16 Å and to R(^{I}C−O) = 1.12 Å. The $G(\mathbf{r})/\rho(\mathbf{r}_c)$ versus R(C−O) bonded interactions obtained in the study of several transition-metal carbonyl clusters[8] fall along the R(C−O) versus $G(\mathbf{r})/\rho(\mathbf{r}_c)$ trend displayed in Figure 1b. Accordingly, as the ratio increases in value for a given bonded interaction, R(M−O) and ν_M both decrease.

The increase in the $G(\mathbf{r})/\rho(\mathbf{r}_c)$ ratio with decreasing R(M−O) and ν_M is consistent with the famous Mooser−Pearson[24] separation diagrams for M_iX_j (i, j = 1−3; M = Na, Mg, Ca, Be, etc.; X = Cl, O, S, C, etc.) normal valence solid-state materials on the basis of the average principal quantum numbers, $\langle n \rangle$, of the valence shells of the bonded atoms and the electronegativity differences, $\Delta\chi$, for the bonded pair. It was assumed that as $\Delta\chi$ and $\langle n \rangle$ both increase, the atomic orbitals comprising a bonded interaction become more poorly developed and lose their directed properties as the bonded interactions change from shared to closed-shell. When scatter diagrams of $\langle n \rangle$ versus $\Delta\chi$ were prepared, the bonded interactions were partitioned largely into disjoint domains, populated with structures with different coordination numbers. The ones with four-coordinated atoms with more directed shared bonded interactions were found to consist of atoms with smaller $\langle n \rangle$ and $\Delta\chi$ values than those populated with structures with six-coordinated atoms. Further, those populated with structures with six-coordinate atoms were found in turn to involve atoms with smaller $\langle n \rangle$ and $\Delta\chi$ values than those for structures with eight-coordinate M atoms. As such, the more open structures with atoms with smaller coordination numbers such as cubic boron nitride, $^{IV}B^{IV}N$, for example, were indicated to consist of shared bonded pairs of atoms with directed bonded interactions whereas the more densely packed structures such as cesium chloride, $^{VIII}Cs^{VIII}Cl$, with larger coordination numbers were indicated to consist of more poorly directed closed-shell bonded interactions.

In a highly cited follow-up paper on the "ionicity" of the chemical bond on the basis of dielectric theory, Phillips[25] generated a spectroscopic-based "covalent energy gap versus ionic energy gap" separation diagram for M^nX^{8-n} tetrahedrally coordinated semiconductors and crystals with octahedrally coordinated rock salt structures that shows that the tetrahedrally coordinated structures with shorter bond lengths are characterized by large "covalent energy gaps" and the octahedrally coordinated rock salt structures are characterized by large "ionic energy gaps". On the basis of $\langle n \rangle$ versus $\Delta\chi$ and the energy gap separation diagrams, it was concluded that substantial "covalent character" favors the formation of less dense open structures with four-coordinated atoms with well-directed bonded interactions whereas high ionicity favors the formation of dense closely packed structures with six-and eight-coodinated atoms. More recently, the decrease in the bond length with decreasing coordination number was firmly established for the M−O bonded interactions for a larger number of oxide materials by Shannon and Prewitt.[26] With these results, the decrease of R(M−O) and ν_M with the increasing $G(\mathbf{r})/\rho(\mathbf{r}_c)$ ratio displayed

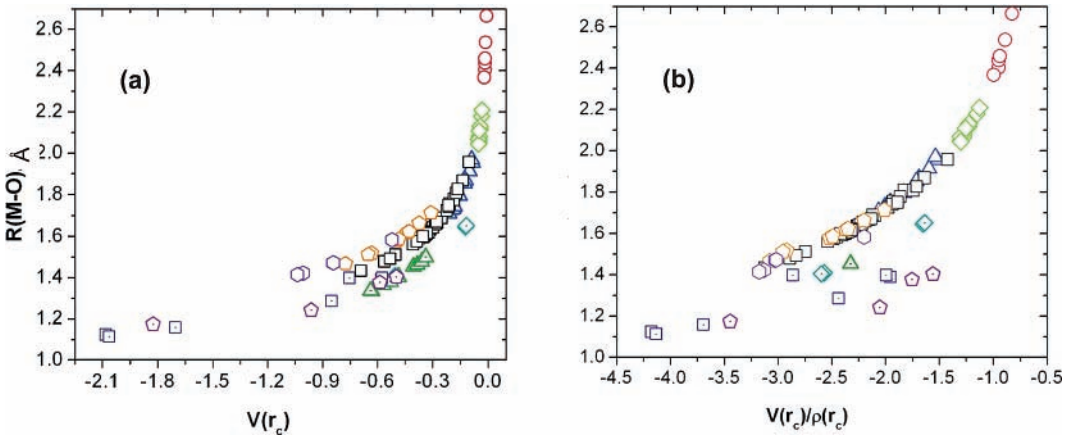

Figure 2. Scatter diagrams of the observed bond lengths, R(M−O) Å, for a relatively large number of earth materials and geometry optimized bond lengths for molecules with C−O and N−O bonded interactions plotted against (a) the local potential energy $V(\mathbf{r}_c)$, (au) and (b) $V(\mathbf{r}_c)/\rho(\mathbf{r}_c)$. See Figure 1 legend for a definition of the symbols.

in Figure 1b conforms with a trend of increasing shared rather than increasing closed-shell interaction.[27,28]

The capacity of the $G(\mathbf{r})/\rho(\mathbf{r}_c)$ ratio to categorize the data for each given bonded interaction into largely disjoint trending domains (Figure 1b) suggests that the ratio is connected to the extent to which the shared component of a bonded interaction is developed. The greater the value of the $G(\mathbf{r})/\rho(\mathbf{r}_c)$, the shorter the bond length, the smaller the value of ν_M, the larger the value of $\rho(\mathbf{r}_c)$, the greater the strength of a given bonded interaction, and the greater the shared component of the bonded interaction. On the basis of these results, the assumption that the ratio $G(\mathbf{r})/\rho(\mathbf{r}_c)$ is less than unity for shared interactions and greater than unity for closed-shell interactions does not appear to hold for the M−O interactions for the earth materials examined in this study, but the converse appears to hold.

Figure 2a and 2b shows that the local potential energy density, $V(\mathbf{r}_c)$, decreases nonlinearly for each bonded interaction with several nonlinear trends displayed for the bonded interactions that are shorter than ∼1.6 Å. As expected, $V(\mathbf{r}_c)$ decreases at a faster rate than $G(\mathbf{r}_c)$ increases for all of the bonded interactions except for the Na−O and Mg−O interactions for which $G(\mathbf{r}_c) > |V(\mathbf{r}_c)|$. Unlike the local kinetic energy density, plotting R(M−O) against the ratio $V(\mathbf{r}_c)/\rho(\mathbf{r}_c)$ results in trends similar to those displayed by plotting R(M−O) against $V(\mathbf{r}_c)$. Since $G(\mathbf{r}_c) > |V(\mathbf{r}_c)|$ for the Na−O and Mg−O bonded interactions, the electronic energy density values, $H(\mathbf{r}_c)$, must necessarily be positive for these interactions. According to Cremer and Kraka,[2] these bonded interactions are indicated to be closed-shell whereas the remaining bonded interactions with negative $H(\mathbf{r}_c)$ values are indicated to be shared with varying degrees of shared character. The $\nabla^2\rho(\mathbf{r}_c)$ values for all of the bonded interactions are positive, except for N−O and several C−O interactions. Indeed, $\nabla^2\rho(\mathbf{r}_c)$ is positive and increases regularly for second-row bonded interactions from ∼4.5 e/Å^5 for the Na−O bonded interaction to ∼ 15 e/Å^5 for the S−O interaction as the value of $\rho(\mathbf{r}_c)$ increases from 0.15 e/Å^3 to 1.90 e/Å^3. Rather than decreasing and becoming progressively more negative as $\Delta\chi$ decreases, $\nabla^2\rho(\mathbf{r}_c)$ is positive and actually increases in value.[29] As asserted by Coppens,[6] negative $\nabla^2\rho(\mathbf{r}_c)$ values, typical for shared bonded interactions between first-row bonded atoms, may not be typical for a shared bonded interaction involving second-row atoms such as Si bonded to O. However, as the coordination number of the Si atom decreases from six to four and the Si−O bond length decreases from 1.76 Å to 1.62 Å for $^{VI}SiO_6$ and $^{IV}SiO_4$ coordination polyhedra, respectively, the distance between the critical point and the nodal surface decreases from 0.40 Å to 0.15 Å, indicating that the bonded interactions comprising a $^{IV}SiO_4$ polyhedron is intermediate in character and that the shared character of Si−O increases as both the coordination number and bond length decrease.[27] In addition, the net atomic charge (+3.17e) conferred on the ^{IV}Si atom in forsterite, Mg_2SiO_4, is smaller than that (+3.39 e) conferred on the ^{VI}Si atom in silica polymorph stishovite, further evidence that the shared character for the ^{IV}Si−O bonded interaction is greater than that for the ^{VI}Si−O bonded interaction.[13] The relationship between the distance between $\mathbf{r}_c$ and the nodal surface has not been examined to our knowledge for the remaining second row M−O interactions.

Figure 3a shows that the local electronic energy density $H(\mathbf{r}_c)$ tends to decrease with decreasing M−O bond lengths as expected from the trends displayed in Figures 1a and 2a and as calculated for the M−O and M−N bonded interactions for the molecules studied by Hill et al.,[30] Feth et al.,[31] and Gibbs et al.[19,32,33] The decrease in $H(\mathbf{r}_c)$ is relatively small for the M−O bonded interaction involving the more electropositive M atoms (Figure 3a), but it decreases more rapidly for the interactions involving the more electronegative atoms. The small positive $H(\mathbf{r}_c)$ values for the Na−O and Mg−O interactions can be explained in terms of the small magnitudes of $G(\mathbf{r}_c)$ and $V(\mathbf{r}_c)$, both of which approach zero as the bonds adopt lengths of 1.75 Å and longer. As the $G(\mathbf{r}_c)$ values for the two interactions are slightly larger than the magnitudes of their $V(\mathbf{r}_c)$ values, the $H(\mathbf{r}_c)$ values for all three are small and positive, also indicating that they are closed-shell.[2] For the remaining interactions, the magnitude of $V(\mathbf{r}_c)$ exceeds that of $G(\mathbf{r}_c)$, with the magnitude of $V(\mathbf{r}_c)$ increasing at a substantially faster rate than $G(\mathbf{r}_c)$ increases with decreasing bond length, and hence $H(\mathbf{r}_c)$ decreases substantially with decreasing bond length. For example, $H(\mathbf{r}_c)$ decreases from −0.41 au to −0.97 au as the bond lengths shorten from ∼1.40 Å for the single C−O bonded interaction for the H_4CO_4 molecule to ∼1.12 Å for the triple C≡O interaction for the CO molecule.

The bonded interactions comprising Figure 3a appear to be organized in linearly trending domains, particularly for the interactions involving the more electropositive M atoms. For example, the Na−O interactions are organized along one, the Mg−O interactions are organized along a second, the Al−O interactions are organized along a third, and so on. When R(M−O) is plotted against the $H(\mathbf{r})/\rho(\mathbf{r}_c)$ ratio, the organization of the bonded interactions into largely disjoint linear domains is more pronounced (Figure 3b). The fact that $H(\mathbf{r}_c)/\rho(\mathbf{r}_c)$ can be used to organize the bonded interactions into such domains, as

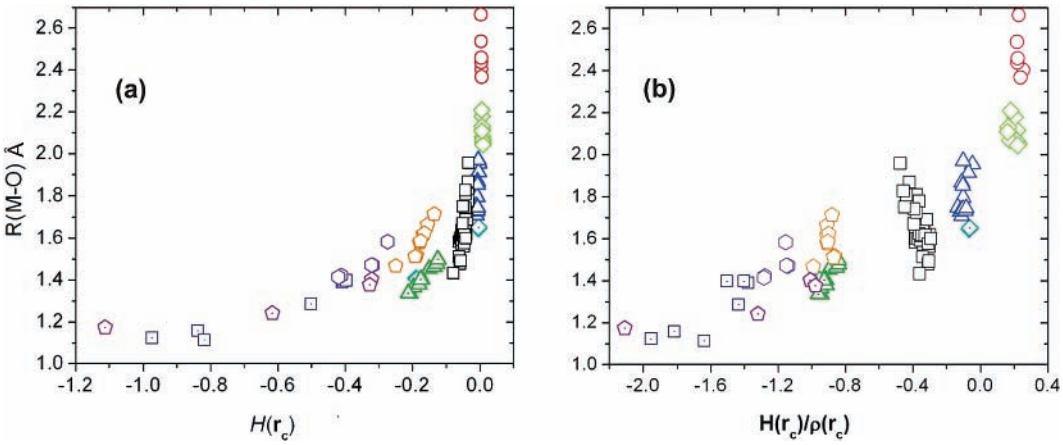

Figure 3. Scatter diagrams of the observed bond lengths, R(M−O) Å, for a relatively large number of earth materials and geometry optimized bond lengths for molecules with C−O and N−O bonds plotted against (a) the local electronic energy density, $H(\mathbf{r}_c)$ (au) where $H(\mathbf{r}_c) = G(\mathbf{r}_c) + V(\mathbf{r}_c)$ (b), $H(\mathbf{r}_c)/\rho(\mathbf{r}_c)$. See Figure 1 legend for a definition of the symbols.

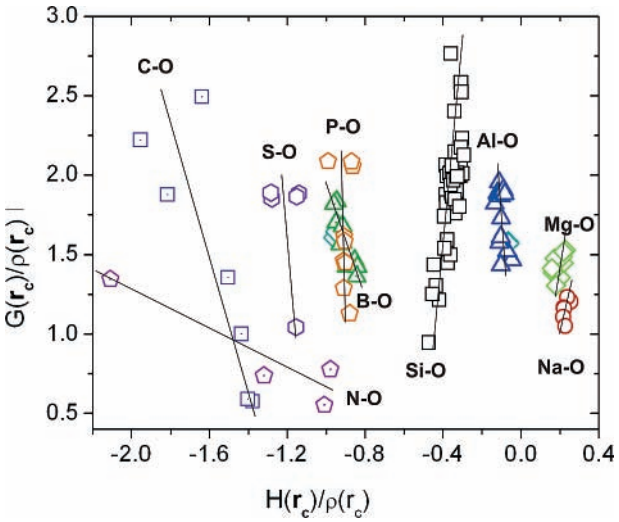

Figure 4. Scatter diagram of $G(\mathbf{r}_c)/\rho(\mathbf{r}_c)$ vs $H(\mathbf{r}_c)/\rho(\mathbf{r}_c)$ where $G(\mathbf{r}_c)$ is the local kinetic energy density, $H(\mathbf{r}_c)$ is the local electronic energy density, and $\rho(\mathbf{r}_c)$ is the value of $\rho(\mathbf{r})$ at $\mathbf{r}_c$. See Figure 1 legend for a definition of the symbols.

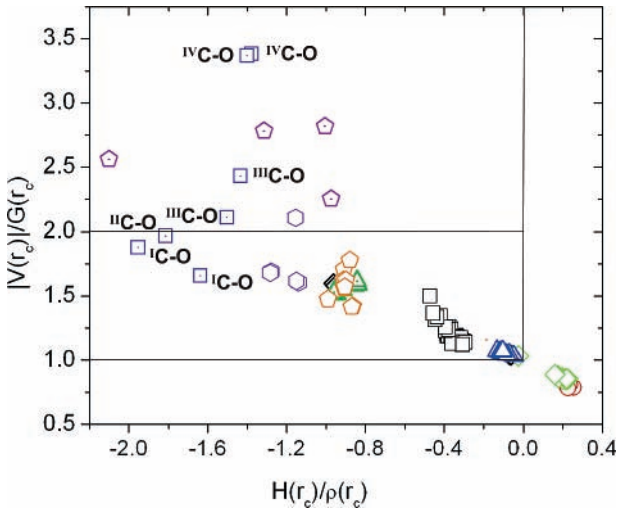

Figure 5. A scatter diagram of the "bond degree" ratio, $|V(\mathbf{r}_c)|/G(\mathbf{r}_c)$ vs $H(\mathbf{r}_c)/\rho(\mathbf{r}_c)$. According to Espinosa et al.,[3] the bonds that fall in the interval $1 < |V(\mathbf{r}_c)|/G(\mathbf{r}_c) < 2$ are classified as intermediate-bonded interactions, those in the interval $0 < |V(\mathbf{r}_c)|/G(\mathbf{r}_c) \leq 1$ are closed-shell interactions, and those with $2 \leq |V(\mathbf{r}_c)|/G(\mathbf{r}_c)$ are shared interactions. The coordination numbers of the carbon atoms are specified by Roman numeral superscripts. For example, ^{III}C−O denoted the C−O bonded interaction comprising the CO_3 anion in calcite, $CaCO_3$. The coordination number of the C atom increases with increasing $|V(\mathbf{r}_c)|/G(\mathbf{r}_c)$ vs $H(\mathbf{r}_c)/\rho(\mathbf{r}_c)$. See Figure 1 legend for a definition of the symbols.

displayed in Figure 3b, suggests that the ratio is connected to some intrinsic property of a given bonded interaction such as $\Delta\chi$, particularly given that the shared bonded interaction is indicated to increase as $H(\mathbf{r}_c)$ decreases and becomes more negative in value.[2,3]

With the observation that the ratios $G(\mathbf{r})/\rho(\mathbf{r}_c)$ and $H(\mathbf{r})/\rho(\mathbf{r}_c)$ can be used to organize the bonded interactions into largely linear trending domains when plotted against R(M−O), a scatter diagram of $G(\mathbf{r})/\rho(\mathbf{r}_c)$ versus $H(\mathbf{r})/\rho(\mathbf{r}_c)$ was prepared to examine whether the bonded interactions can be likewise organized into linear trending domains as displayed in Figure 4. From the bottom to the top in the figure, R(M−O) and ν_M both decrease, $\rho(\mathbf{r}_c)$ and λ_3 both increase, and the strengths and directed properties of the bonded interactions are indicated to increase in each domain as the $G(\mathbf{r})/\rho(\mathbf{r}_c)$ ratio increases in value. Albeit not perfect, the ratio $H(\mathbf{r})/\rho(\mathbf{r}_c)$ orders the bonded interactions into separate linear domains from right to left in the figure as $\Delta\chi$ decreases.[20] With a few exceptions, $\Delta\chi$ decreases from right to left in the figure in the order Na−O, $\Delta\chi = 2.74$; Mg−O, $\Delta\chi = 2.32$; Al−O, $\Delta\chi = 2.00$; Si−O, $\Delta\chi = 1.69$; B−O, $\Delta\chi = 1.56$; P−O, $\Delta\chi = 1.36$; S−O, $\Delta\chi = 1.02$; C−O, $\Delta\chi = 1.07$; N−O, $\Delta\chi = 0.54$. The N−O bonded interactions display a strikingly different trend than that displayed by the other interactions, a feature that may be related to the negative $\nabla^2\rho(\mathbf{r}_c)$ values calculated for the N−O interactions.

As observed above, it was proposed[3] that bonded interactions can be classified on the basis of the $|V(\mathbf{r}_c)|/G(\mathbf{r}_c)$ ratio with a bonded interaction defined as a closed-shell when the ratio $|V(\mathbf{r}_c)|/G(\mathbf{r}_c) < 1$, shared when $|V(\mathbf{r}_c)|/G(\mathbf{r}_c) > 2$, and intermediate when the ratio falls between 1 and 2. As the ratio $|H(\mathbf{r}_c)|/\rho(\mathbf{r}_c)$ appears to be connected to $\Delta\chi$, a scatter of $|V(\mathbf{r}_c)|/G(\mathbf{r}_c)$ versus $H(\mathbf{r}_c)/\rho(\mathbf{r}_c)$ was prepared (Figure 5).[11] The ratios for the M−O bonded interactions scatter along the diagonal of the figure as $\Delta\chi$ decreases with decreasing $H(\mathbf{r}_c)/\rho(\mathbf{r}_c)$ with the Na−O, Be−O, and Mg−O bonded interactions classifying as closed-shell and the Al−O, Si−O, B−O, and P−O interactions classifying as intermediate interactions. The C−O bonded interactions that fall in the intermediate $|V(\mathbf{r}_c)|/G(\mathbf{r}_c)$ region between 1 and 2 are the ones with multiple bonds with $|V(\mathbf{r}_c)|/G(\mathbf{r}_c)$ ratios ranging between 1.66 and 1.97 while the remaining single C−O bonded interactions with ratios greater than 2 classify as shared. In short, the $|V(\mathbf{r}_c)|/G(\mathbf{r}_c)$ ratio indicates that

the shared character for the C−O bonded interaction increases from the triple $^{I}C{\equiv}O$ bonded interaction for carbon monoxide to the double $^{II}C{=}O$ interaction for the carbon dioxide molecule to the single $^{IV}C-O$ interactions in the H_4CO_4 molecule, contrary to the trend between $H(\mathbf{r}_c)$, ν_M, and shared bonded interaction discussed above. It is also contrary to the σ-orbital rule that the electronegativity (highest to the lowest electronegativity) decreases in the order $sp > sp^2 > sp^3$ with the greater the percentage of s-character, the larger the electronegativity.[21] As the s-character for the triple $^{I}C{\equiv}O$ bonded interaction (smaller $\Delta\chi$) is greater than that for a single C−O interaction, the σ-orbital rule indicates that the $^{I}C{\equiv}O$ interaction is a more shared interaction than that for the $^{IV}C-O$ interaction, contrary to placing of the single-bonded interactions in the shared region of Figure 5 and placing the triple interaction in the intermediate region.[13,34] On the whole, for the M−O bonded interactions considered in this study, the ratio $|V(\mathbf{r}_c)|/G(\mathbf{r}_c)$ appears to do an adequate job classifying the bonded interactions involving the more electropositive M atoms, but it appears to be inadequate for the bonded interactions involving the more electronegative M atoms and a variety of coordination numbers.

Expectation Values for Local Energy Density Properties. Given that almost all recent experimental electron density analyses report bond critical point properties, to our knowledge, there is no straightforward way of obtaining the local energy density properties from an experimental electron density distribution. However, $G(\mathbf{r})$ can be estimated with the gradient-corrected electron gas theory approximation $\langle G(\mathbf{r})\rangle = (3/10)(3\pi^2)^{2/3}\rho^{5/3}(\mathbf{r}) + \lambda[\nabla\rho(\mathbf{r})]^2/\rho(\mathbf{r}) + 1/6\nabla^2\rho(\mathbf{r})$.[35] At a bond critical point where $\nabla\rho(\mathbf{r}) = 0$, the expression reduces to $\langle G(\mathbf{r}_c)\rangle = (3/10)(3\pi^2)^{2/3}\rho^{5/3}(\mathbf{r}_c) + 1/6\nabla^2\rho(\mathbf{r}_c)$. With the experimental values for $\rho(\mathbf{r}_c)$ and $\nabla^2\rho(\mathbf{r}_c)$, $\langle G(\mathbf{r}_c)\rangle$ can be evaluated at the bond critical point with varying degrees of success. With $\langle G(\mathbf{r}_c)\rangle$ and the local virial equation, an estimate of the local potential energy density, $V(\mathbf{r}_c)$, can also be made using the expession $\langle V(\mathbf{r}_c)\rangle = 1/4\nabla^2\rho(\mathbf{r}_c) - 2\langle G(\mathbf{r}_c)\rangle$.[22] With the estimates of $\langle V(\mathbf{r}_c)\rangle$ and $\langle G(\mathbf{r}_c)\rangle$, the ratio $|\langle V(\mathbf{r}_c)\rangle|/\langle G(\mathbf{r}_c)\rangle$, for example, can be determined. The accuracy with which $\langle V(\mathbf{r}_c)\rangle$ and $\langle G(\mathbf{r}_c)\rangle$ can be determined is highly dependent on the accuracy with which $\rho(\mathbf{r}_c)$ and $\nabla^2\rho(\mathbf{r}_c)$ are determined in a multipole modeling of $\rho(\mathbf{r})$. Further, the estimated values for $\langle V(\mathbf{r}_c)\rangle$ and $\langle G(\mathbf{r}_c)\rangle$ will necessarily reflect model-dependent errors as well as the validity of the approximation. As observed above, if accurate experimental values for $\rho(\mathbf{r}_c)$ and $\nabla^2\rho(\mathbf{r}_c)$ are known, then semiquantitative to quantitative expectation values, $\langle G(\mathbf{r}_c)\rangle$ and $\langle V(\mathbf{r}_c)\rangle$ for $G(\mathbf{r}_c)$ and $V(\mathbf{r}_c)$, can be obtained.

The $\langle G(\mathbf{r}_c)\rangle$ and $\langle V(\mathbf{r}_c)\rangle$ values generated for several diatomic molecules were found by Abramov[22] to agree typically within ~5%, on average, with those calculated, whereas the agreement for several hydrocarbon molecules was found to be substantially poorer, within ~35%. In a later study, $\rho(\mathbf{r})$ was calculated in an evaluation of the bond critical point and the local energy density properties for ~40 H···F closed-shell interactions.[36] With the theoretical values for $\rho(\mathbf{r}_c)$ and $\nabla^2\rho(\mathbf{r}_c)$, the gradient-corrected electron gas theory approximation and the local virial expression, $\langle G(\mathbf{r}_c)\rangle$, was determined and found to be highly correlated with the values of $G(\mathbf{r}_c)$, closely following the 45° line with a coefficient of determination of 0.998. With the electron density distribution generated for $Mn_2(CO)_{10}$, Farrugia et al.[5] found that $\langle G(\mathbf{r}_c)\rangle$ and $\langle V(\mathbf{r}_c)\rangle$ are also in good agreement with those calculated at BLYP/6-311+G* level.

In addition, Knop et al.[37] geometry optimized the structures for ~50 small molecules containing linear or near-linear N−H···N bonded interactions and found that values of $\langle G(\mathbf{r}_c)\rangle$, generated with the $\rho(\mathbf{r}_c)$ and $\nabla^2\rho(\mathbf{r}_c)$ values for the molecules, approximate $G(\mathbf{r}_c)$ very well for the weaker H···N interactions with $G(\mathbf{r}_c)$ values less than 0.02 au. For the stronger H···N bonded interactions, the values of $\langle G(\mathbf{r}_c)\rangle$ likewise correlate with $G(\mathbf{r}_c)$ values, but they depart from the 45° line and become progressively larger as $G(\mathbf{r}_c)$ increases to 0.06 au beyond which the trend is lost. Despite that $\nabla\rho(\mathbf{r}) \neq 0$ in the spatial intermolecular region, Galvez et al.[38] found that the truncated gradient-corrected electron gas theory approximation can be reliably used in this region and along the bond paths to generate accurate estimates of $\langle G(\mathbf{r}_c)\rangle$ for $(HF)_2$ and $(H_2O)_2$ dimers. However, as expected, the approximation yielded unreliable values for those regions in close proximity with the atomic nuclei where $\nabla\rho(\mathbf{r})$ is typically very large.

Each of these studies lend support to Abramov's strategy[22] for estimating the local energy density properties for a material with the Galvez et al.[38] study demonstrating the usefulness of $\langle G(\mathbf{r}_c)\rangle$ for studies of intermolecular interactions in terms of $\rho(\mathbf{r})$ and $\nabla^2\rho(\mathbf{r})$. Further, in the case where $\mathbf{r}_c$ is in close proximity or intersects the $\nabla^2\rho(\mathbf{r}_c)$ nodal plane at a point where $\nabla(\nabla^2\rho(\mathbf{r}))$ is very large, for example, as reported for the $^{I}C{\equiv}O$ bonded interaction in carbon monoxide,[8] the determination of $\nabla^2\rho(\mathbf{r}_c)$ can result in a substantial error. As such, the determination of $\langle G(\mathbf{r}_c)\rangle$ and $\langle V(\mathbf{r}_c)\rangle$ may be necessarily inaccurate. Further, if the position of $\mathbf{r}_c$ is not located accurately in a theoretical study, the errors in the expectation values may also be large.[12] Also, a large error in $\nabla^2\rho(\mathbf{r}_c)$ can lead to an unsatisfactory classification of a bonded interaction on the basis of the value of $H(\mathbf{r}_c)$, for example.

In a determination of how well the expectation values, $\langle G(\mathbf{r}_c)\rangle$ and $\langle V(\mathbf{r}_c)\rangle$, obtained with the theoretical $\rho(\mathbf{r}_c)$ and $\nabla^2\rho(\mathbf{r}_c)$ values generated in this study reproduce $G(\mathbf{r}_c)$ and $V(\mathbf{r}_c)$, respectively, Figure 6 was constructed. The agreement between the expectation and the theoretical values for the second-row M−O bond interactions displayed in Figures 1a and 2a is good. On the other hand, the agreement is poorer for the stronger first-row shared C−O and N−O bonded interactions. Abramov[22] likewise found poorer agreement for the stronger shared bonded interactions for the hydrocarbons. Likewise, as observed above, Knop et al.[37] found poorer agreement for the stronger H···N bonded interactions. Despite the potential problem encountered in determining the Laplacian for carbon monoxide, the values $\langle G(\mathbf{r}_c)\rangle$ and $\langle V(\mathbf{r}_c)\rangle$ obtained in this study are in reasonably good agreement with the theoretical $G(\mathbf{r}_c)$ and $V(\mathbf{r}_c)$ values, particularly for the second-row M−O bonds.

To establish how well the $\langle G(\mathbf{r}_c)\rangle$ and $\langle V(\mathbf{r}_c)\rangle$ data reproduce the trends in Figures 1b and 4, the ratios $\langle G(\mathbf{r}_c)\rangle/\rho(\mathbf{r}_c)$ and $\langle H(\mathbf{r}_c)\rangle/\rho(\mathbf{r}_c)$ were calculated and plotted in Figure 7a and 7b, respectively. The scatter of the bonded interaction data in Figure 1b and Figure 4 is similar to that displayed in Figure 7b and 7a, respectively. The linear trends for the second-row bonds are likewise strikingly similar with those displayed by the theoretical data. As expected, the trends displayed by the C−O, and particularly by the N−O bonded interaction data in the two figures, differ somewhat from the theoretical trends. All in all, it is clear that the Abramov[22] use of the local kinetic energy density estimate provides quantitative estimates of $G(\mathbf{r}_c)$, particularly for second-row M−O and the B−O bonded interactions, but a less quantitative estimate for first-row N−O and C−O bonded interactions, both of which display negative $\nabla^2\rho(\mathbf{r}_c)$ values.

Concluding Remarks

The Bader−Essén[1] strategy for classifying bonded interactions not only has the merits of being relatively simple and straight-

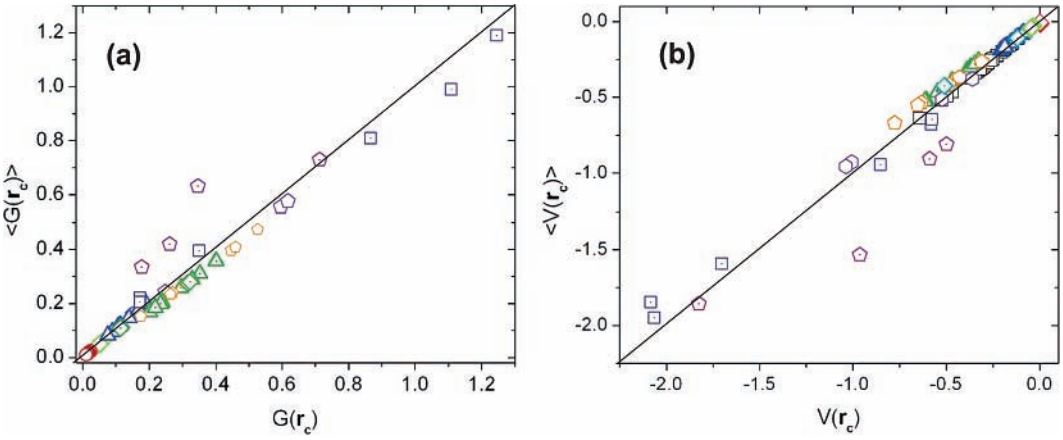

Figure 6. A comparison of (a) the estimated value of $\langle G(\mathbf{r}_c)\rangle$ vs the theoretical value of $G(\mathbf{r}_c)$ and (b) the estimated value of $\langle V(\mathbf{r}_c)\rangle$ vs the theoretical value of $V(\mathbf{r}_c)$. $G(\mathbf{r}_c)$ was estimated with the approximation $\langle G(\mathbf{r}_c)\rangle = (3/10)(3\pi^2)\rho^{5/3}(\mathbf{r}_c) + 1/6\nabla^2\rho(\mathbf{r}_c)$ and $V(\mathbf{r}_c)$ was estimated with the expression $\langle V(\mathbf{r}_c)\rangle = 1/4\nabla^2\rho(\mathbf{r}_c) - 2\langle G(\mathbf{r}_c)\rangle$. See Figure 1 legend for a definition of the symbols.

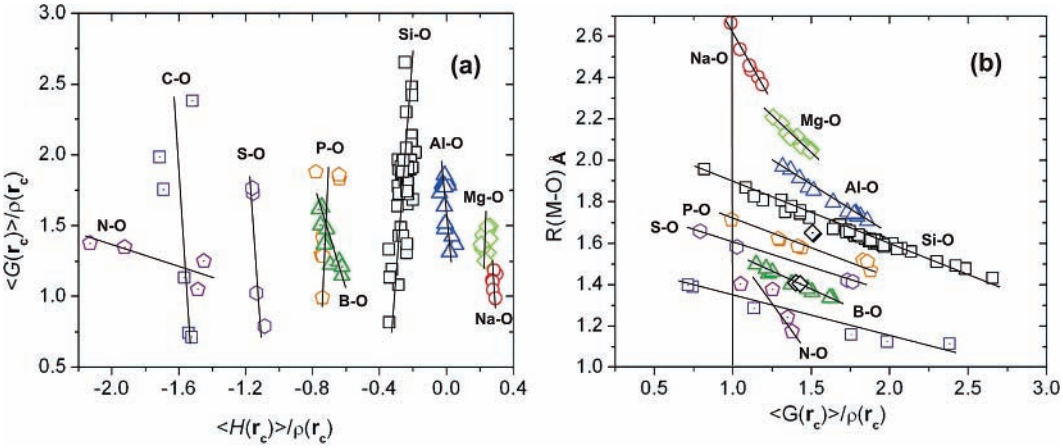

Figure 7. (a) Scatter diagram of $\langle G(\mathbf{r}_c)\rangle/\rho(\mathbf{r}_c)$ vs $\langle H(\mathbf{r}_c)\rangle/\rho(\mathbf{r}_c)$ where $\langle G(\mathbf{r}_c)\rangle$ is the expectation value of the local kinetic energy density, and $\langle H(\mathbf{r}_c)\rangle$ is the expectation value of the local electronic energy density, and $\rho(\mathbf{r}_c)$ is the value of $\rho(\mathbf{r})$ at $\mathbf{r}_c$. (b) Scatter diagram of R(M−O) vs the ratio $\langle G(\mathbf{r}_c)\rangle/\rho(\mathbf{r}_c)$. See Figure 1 legend for a definition of the symbols.

forward, but it has been used with considerable success in advancing our understanding of the bonded interactions for a wide range of materials. However, for materials with 3d transition-metal atoms, the strategy has been found to be inadequate in the classification of the bonded interactions because the valence shell charge concentrations of $\rho(\mathbf{r})$ are often poorly developed and the signs of $\nabla^2\rho(\mathbf{r}_c)$ are largely indeterminate,[9] indicating that they may well represent a separate class of bonded interactions.[39]

The strategy based on the bond index $|V(\mathbf{r}_c)|/G(\mathbf{r}_c)$ ratio[3] has been found to be a useful and adequate strategy for a variety of bonded interactions with closed-shell, shared, and transition-metal atom interactions. For example, Bianchi et al.[40] and Gervasio et al.[41] observed that the ratio seems to provide a powerful strategy for characterizing and classifying a variety of interactions, including metal−metal interactions.Yet, as observed above, the ratio does not appear to manifest changes in the M−O interactions related to changes in the coordination number and the net atomic charges of the M atoms.

Of the three classifications, the use of the sign and magnitude of $H(\mathbf{r}_c)$ appears to be adequate for classifying the M−O bonded interactions for earth materials. Unlike the $|V(\mathbf{r}_c)|/G(\mathbf{r}_c)$ ratio, $H(\mathbf{r}_c)$ seems to provide a more consistent measure of how the character of the interactions changes with the coordination number and the net charges of the bonded atoms.[12] It even provides a classification of transition metal−metal bonds that is in keeping with the character of the shared bonded interactions. However, it can display a substantial error when estimated with experimental $\nabla^2\rho(\mathbf{r}_c)$ values, but it appears to be the most universal and adequate of the three classifications at this time.

Finally, the scatter diagram of $G(\mathbf{r}_c)/\rho(\mathbf{r}_c)$ versus $H(\mathbf{r}_c)/\rho(\mathbf{r}_c)$ ratio serves to categorize the M−O bonded interactions for the earth materials examined in this study into linear domains that appear to be connected to $\Delta\chi$, the greater the value of $H(\mathbf{r}_c)/\rho(\mathbf{r}_c)$, the smaller the value of $\Delta\chi$. Further, within the domains, $G(\mathbf{r}_c)/\rho(\mathbf{r}_c)$ increases as R(M−O), ν_M, and $H(\mathbf{r}_c)$ each decrease and $\rho(\mathbf{r}_c)$ increases. It will be of interest to see whether interactions involving transitional-metal atoms bonded to O and metal−metal interactions can be classified accordingly. However, as the range in the M−O bond lengths displayed by transition-metal atoms is typically smaller than those displayed by non-transition-metal atoms, the R(M−O) versus $G(\mathbf{r}_c)/\rho(\mathbf{r}_c)$ trends, for example, will likely display a smaller range of values.[26]

Acknowledgment. The National Science Foundation and the U.S. Department of Energy are thanked for supporting this study in part with Grants EAR-0609885 (N.L. Ross and G.V.G.), DE-FG02-03ER15389 (J.D. Rimstidt and G.V.G.), and DE-FG02-97ER14751 (D.F.C.). G.V.G. wishes to thank the Gledden Foundation for generously providing support for his visit to the University of Western Australia with a Gledden Senior Fellowship. He also wishes to thank Mark Spackman for nominating him for the Fellowship. He also wishes to thank Virginia

Tech for providing additional support for the visit. K.M.R. acknowledges support from the Environmental Molecular Sciences Laboratory (EMSL) at the Pacific Northwest National Laboratory (PNNL). The computations were performed in part at the EMSL at PNNL. The EMSL is a national scientific user facility sponsored by the U.S. DOE's Office of Biological and Environmental Research. PNNL is operated by Battelle for the DOE under Contract DE-AC06-76RLO 1830.

References and Notes

(1) Bader, R. F. W.; Essen, H. *J. Chem. Phys.* **1984**, *80*, 1943.
(2) Cremer, D.; Kraka, E. *Croat. Chem. Acta* **1984**, *57*, 1259.
(3) Espinosa, E.; Alkorta, I.; Elguero, J.; Molins, E. *J. Chem. Phys.* **2002**, *117*, 5529.
(4) Gatti, C. *Z. Kristallogr.* **2005**, *220*, 399.
(5) Farrugia, L. J.; Frampton, C. S.; Howard, J. A. K.; Mallinson, P. R.; Peacock, R. D.; Smith, G. T.; Stewart, B. *Acta Crystallogr., Sect. B* **2006**, *62*, 236.
(6) Coppens, P. *X-ray Charge Densities and Chemical Bonding*; Oxford University Press: Oxford, U.K., 1997.
(7) Koritsanszky, T. S.; Coppens, P. *Chem. Rev.* **2001**, *101*, 1583.
(8) Macchi, P.; Sironi, A. *Coord. Chem. Rev.* **2003**, *238*−*239*, 383.
(9) Gatti, C.; Bertini, L.; Cargnoni, F. *Acta Crystallogr.* **2005**, *A61*, C47.
(10) Bianchi, R.; Gatti, C.; Adovasio, V.; Nardelli, M. *Acta Crystallogr., Sect. B* **1996**, *52*, 471.
(11) Marabello, D.; Bianchi, R.; Gervasio, G.; Cargnoni, F. *Acta Crystallogr., Sect. A* **2004**, *A60*, 494.
(12) Bianchi, R.; Forni, A.; Oberti, R. *Phys. Chem. Miner.* **2005**, *32*, 638.
(13) Gibbs, G. V.; Cox, D. F.; Crawford, T. D.; Rosso, K. M.; Ross, N. L.; Downs, R. T. *J. Chem. Phys.* **2006**, *124*.
(14) Bader, R. F. W. *Atoms in Molecules*; Oxford Science Publications: Oxford, U.K., 1990.
(15) Saunders, V. R.; Dovesi, R.; Roetti, C.; Causa, M.; Harrison, N. M.; Orlando, R.; Apra, E. *CRYSTAL98 User's Manual*; University of Torino: Torino, Italy, 1998.
(16) Gatti, C. *TOPOND96 User's Manual*; CNR-CSRSRC: Milano, Italy, 1997.
(17) Dirac, P. A. M. *The Principles of Quantum Mechanics*; Oxford University Press: Oxford, U.K., 1958.
(18) Vosko, S. H.; Wilk, L.; Nusair, M. *Can. J. Phys.* **1980**, *58*, 1200.
(19) Gibbs, G. V.; Boisen, M. B.; Beverly, L. L.; Rosso, K. M. A computational quantum chemical study of the bonded interactions in earth materials and structurally and chemically related molecules. In *Molecular Modeling Theory: Applications in the Geosciences*; Cygan, R. T., Kubicki, J. D., Eds.; Mineralogical Society of America: Washington, DC, 2001; Vol. 42, p 345.
(20) Downs, R. T.; Gibbs, G. V.; Boisen, M. B., Jr.; Rosso, K. M. *Phys. Chem. Miner.* **2002**, *29*, 369.
(21) Allen, L. C. *J. Am. Chem. Soc.* **1989**, *111*, 9003.
(22) Abramov, Y. A. *Acta Crystallogr.* **1997**, *A53*, 264.
(23) Ruedenberg, K. *Rev. Mod. Phys.* **1962**, *34*, 326.
(24) Mooser, E.; Pearson, W. B. *Acta Crystallogr.* **1959**, *12*, 1015.
(25) Phillips, J. C. *Rev. Mod. Phys.* **1970**, *42*, 317.
(26) Shannon, R. D.; Prewitt, C. T. *Acta Crystallogr.* **1969**, *B25*, 925.
(27) Bloch, A. N.; Schatteman, G. C. Quantum-Defect Orbital Radii and the Structural Chemistry of Simple Solids. In *Structure and Bonding (Berlin) in Crystals*; O'Keeffe, M., Navrotsky, A., Eds.; Academic Press: New York, 1981; Vol. 1, p 49.
(28) Zunger, A. A Pseudopotential Viewpoint of the Electronic and Structural Properties of Crystals. In *Structure and Bonding (Berlin) in Crystals*; O'Keeffe, M. Navrotsky, A., Eds.; Academic Press: New York, 1981; Vol. 1, p 73.
(29) Kirfel, A.; Lippmann, T.; Blaha, P.; Schwarz, K.; Cox, D. F.; Rosso, K. M.; Gibbs, G. V. *Phys. Chem. Miner.* **2005**, *32*, 301.
(30) Hill, F. C.; Gibbs, G. V.; Boisen, M. B. *Phys. Chem. Miner.* **1997**, *24*, 582.
(31) Feth, S.; Gibbs, G. V.; Boisen, M. B.; Hill, F. C. *Phys. Chem. Miner.* **1998**, *25*, 234.
(32) Gibbs, G. V.; Boisen, M. B., Jr.; Hill, F. C.; Tamada, O.; Downs, R. T. *Phys. Chem. Miner.* **1998**, *25*, 574.
(33) Gibbs, G. V.; Hill, F. C.; Boisen, M. B., Jr. *Phys. Chem. Miner.* **1997**, *24*, 167.
(34) Gatti, C.; Lasi, D. submitted.
(35) Kirzhnits, D. A. *Sov. Phys. JETP* **1957**, *5*, 64.
(36) Espinosa, E.; Alkorta, I.; Rozas, I.; Elguero, J.; Molins, E. *Chem. Phys. Lett.* **2001**, *336*, 457.
(37) Knop, O.; Rankin, K. N.; Boyd, R. J. *J. Phys. Chem. A* **2003**, *107*, 272.
(38) Galvez, O.; Gomez, P. C.; Pacios, L. F. *Chem. Phys. Lett.* **2001**, *337*, 263.
(39) Cortes-Guzman, F.; Bader, R. F. W. *Coord. Chem. Rev.* **2005**, *249*, 633.
(40) Bianchi, R.; Gervasio, G.; Marabello, D. *C. R. Chim.* **2005**, *8*, 1392.
(41) Gervasio, G.; Bianchi, R.; Marabello, D. *Chem. Phys. Lett.* **2004**, *387*, 481.